Eur. J. Mech. B - Fluids 19 (2000) 673–694

S0997-7546(00)00129-1/FLA

Eddy structure in turbulent boundary layers

Julian C.R. Hunt [a,1], Jonathan F. Morrison [b,*]

[a] *Departments of Space and Climate Physics and Geological Sciences, University College, Gower St., London WC1, UK*
[b] *Department of Aeronautics, Imperial College, London SW7 2BY, UK*

(Received 4 October 1999; revised 1 March 2000; accepted 27 March 2000)

Abstract – In this paper a new analysis is proposed for the driving mechanisms and the statistics for turbulent boundary layers at very high Reynolds numbers. It differs from theories for moderate to low Reynolds numbers and is based on the results of (linear) rapid distortion theory, and both laboratory and field experimental data. The large-scale eddy structure near the wall in boundary layers is distorted in several ways: by the strong mean shear, by the blocking of the normal velocity component and by the moving internal shear layers produced by large eddies as they impinge and scrape along the wall. Elongated streamwise vortices are formed with length scales that are several times the boundary layer height. An approximate stability argument suggests that if the Reynolds number for the turbulence, $\mathrm{Re}_\tau \gg 10^4$, these internal layers are fully turbulent and that the large eddies can burst upward where the vortical eddies interact. The forms of the main statistical quantities, such as variances, spectra, length scales, are derived in terms of outer layer quantities using surface similarity and inhomogeneous linear theory. These 'top-down' eddy-impingement, inner-layer/eddy-interaction/ejection mechanisms at very high Reynolds number are sensitive to changes in surface conditions and to variations in pressure gradients. They may therefore require different techniques for their control from those used at lower Reynolds number when boundary layers are driven by 'bottom-up' instability/surface-interaction mechanisms. Furthermore, accurate numerical modelling of boundary layers at high Reynolds number requires resolving surface processes at very fine resolution. By inference, it is likely that there is some residual 'top-down' influence, even at low Re_τ. © 2000 Éditions scientifiques et médicales Elsevier SAS

turbulent boundary layers / rapid distortion theory

1. Introduction

Turbulent boundary layers have a complex structure and a number of characteristic phenomena that are still not well understood, especially for high Reynolds number flows. More notable aspects are: bursts, the frequency of which decreases with increasing Reynolds number; downdrafts, that lead to regions of high velocity near the surface (visible as 'cats paws' at high Reynolds number typically covering about 15% on the sea surface, Scorer [1]), and streamwise rolls ranging in scale from those of small intense surface vortices to those with diameters of the order of that of the boundary layer thickness (Holmes et al. [2], Townsend [3]). The forms of the spectra of the horizontal components of the velocity near the surface are unique to wall flows (i.e. are inversely proportional to the wave number) but further away revert to those of other shear flows (Kader and Yaglom [4], Perry and Marušić [5]). An important question is to what extent these characteristics also occur where there are additional bounding surfaces such as in pipes and channels. A notable feature of boundary layers is that the streamwise intensity continues to increase with Reynolds number apparently without affecting the mean velocity profile. How do the 'inactive' motions (Townsend [6], Bradshaw [7], Morrison et al. [8]) relate to the eddy structure and are they dynamically significant?

* Correspondence and reprints; also at: Department of Mechanical and Aerospace Engineering, Princeton University, D-226 Engineering Quadrangle, Olden Street, Princeton NJ 08544-5263, USA; e-mail: jmorriso@princeton.edu
[1] Also at J.M. Burgers Centre, Delft University of Technology, Delft, The Netherlands

Although investigators tend to agree about the many different fluid dynamic mechanisms that might operate, there is not so much agreement about which are most relevant for explaining the main features of the flow and how their relative significance might change as the Reynolds number varies; see Barenblatt and Chorin [9]. The two most controversial questions concerning mechanisms concerns the role of surface eddy motions as the Reynolds number changes and their coupling with those eddies at the top of the boundary layer (Head and Bandyophadhay [10], Falco [11,12], Schoppa and Hussain [13]).

A practical reason for studying the eddy structure is that it enables us firstly to improve the statistical modelling and sub-grid elements in the numerical simulation of these flows, especially the statistics involving higher order and multi-point correlations. Secondly, it helps us to improve our understanding of how these flows change as a result of external disturbances, such as the introduction of obstacles or free-stream turbulence above the layer.

The aim of this paper is to illustrate the considerable advances in our understanding of the local and non-local mechanisms that affect eddies in idealised inhomogeneous turbulent shear flows, both without and with rigid boundaries. We also suggest how several of these mechanisms operate interactively together to determine the statistics of the velocity field and the eddy structure of turbulent boundary layers. We also consider the distribution of the turbulence throughout the whole layer at very high Reynolds number, as has been studied in the atmosphere as well as in artificially thickened boundary layers, which can have many of the same properties (Hunt and Fernholz [14]). Panton [15] edited an extended review of the restricted range of mechanisms operating very close to the wall at moderate Reynolds numbers (where $u_* h/\nu < 1000$, h is the layer depth, u_* the surface friction velocity and ν the kinematic viscosity).

2. Turbulent eddies near a wall

2.1. Flow structure

A rigid plane boundary, or 'wall', affects any turbulent velocity field generated above it through several mechanisms. *Figure 1* shows a schematic of the high-Reynolds-number boundary layer with freestream velocity, U_E. We define also a 'middle layer' $[M]$, bounded from above by the instantaneous interface $[S_I]$ and from below by an internal shear layer $[S]$ of height h_s, which is essentially the outer limit of the log-law profile. Within this, we define a shear layer generated by eddy/ground interactions and of height $h_e < h_s$. In this 'eddy shear layer' $[ESL]$, we expect some local quasi-energy equilibrium region in the domain $[W]$ with some length scale L_*, such that $h_r < L_* < h_e$, where h_r is the roughness sublayer height.

The simplest case is that of a shear free boundary layer (SFBL), for which the theoretical concepts (cf. Hunt [16]) have been tested by experiments and numerical simulation applied to various kinds of turbulence, such as generated by shear layers above the boundary (Wood and Bradshaw [17]), or by oscillating grids (Thole and Bogard [18]), with typical rms velocity u_E, length scale, L_E, and a mean velocity profile, $U(z)$, above the wall. In the case of a SFBL, $u_E \ll U_E$, where $U_E = U(L_E)$.

2.2. Shear-free boundary layers

2.2.1. Blocking

Consider a vortical eddy (such as a vortex ring or vortex pair) moving with a characteristic velocity u_e, and length scale L_e towards the wall (*figure 2*(*a*)). When the eddy is at a distance $z^e(t=0) \gg L_e$, there is a region of irrotational motion induced by the eddy and its image, but above the vortical surface layer (of thickness h_e),

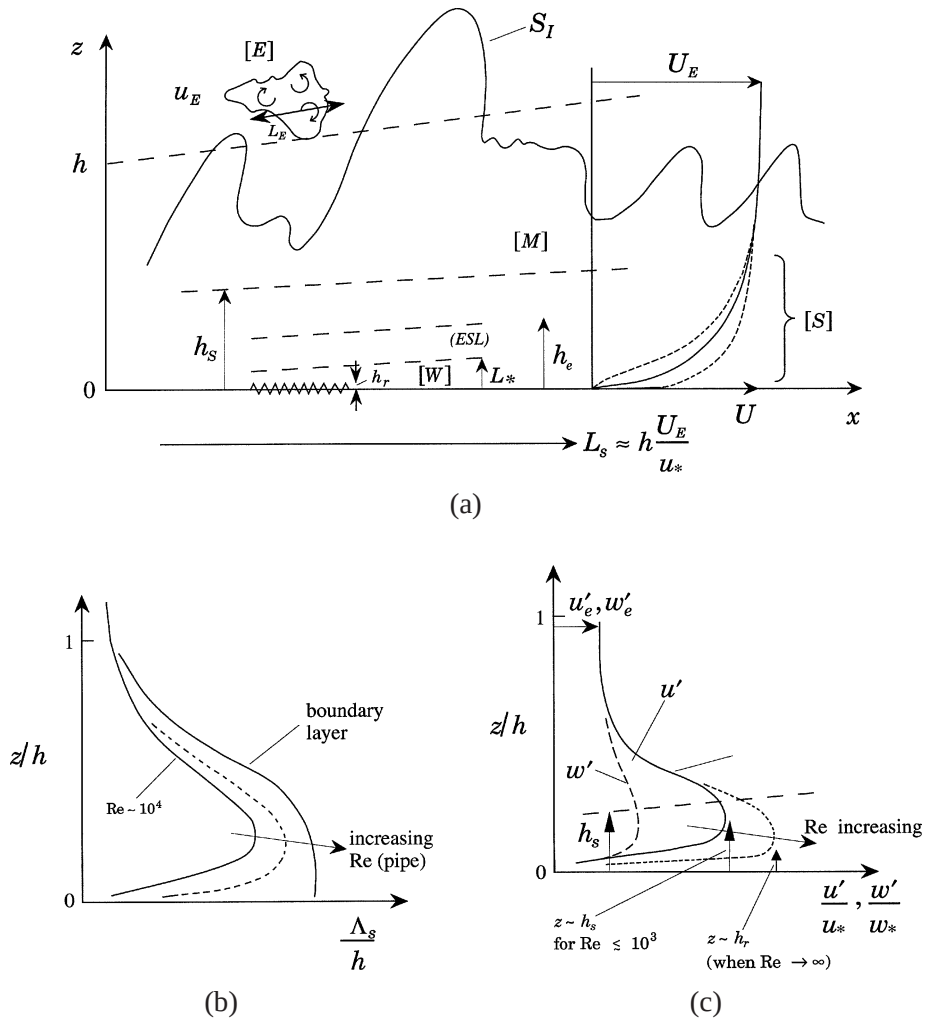

Figure 1. Schematic of boundary layer and principal scales over wide Reynolds number range: (a) instantaneous streamwise velocity profile; (b) $\frac{\Lambda_s}{h}$ *vs.* $\frac{z}{h}$ (typically, $\frac{\Lambda_s}{h}$ in pipe is many times that in boundary layer); (c) turbulent intensities $\frac{u'}{u_*}, \frac{w'}{u_*}$ *vs.* $\frac{z}{h}$.

which we consider in the next section. Where $z^e \gg z > h_e$, the normal and horizontal velocity components are:

$$w \approx \frac{z}{z^e} u_e. \tag{1}$$

Note how the blocking effect of the wall, or the image, reduces w and increases u and that the eddy's own vorticity field may induce it to move closer to the wall and slow down. In general the eddy also moves parallel to the wall, and the velocity may be increased by the image eddy. Collisions with other eddies are an important factor to consider as we show later. The unsteady deformation of the velocity field is also the reason why the pressure induced at the surface by the eddy as it impinges is much less than the dynamic head $\frac{1}{2}\rho u_e^2$. Typically it is of order $\frac{1}{4}$ to $\frac{1}{3}$ of this value (Hunt and Durbin [19]).

The eddy analysis explains the behaviour of a fully turbulent flow near a rigid boundary where the turbulence is continuously generated in the 'freestream' above it; see *figure 3*. Outside the surface layer, the mean rate of

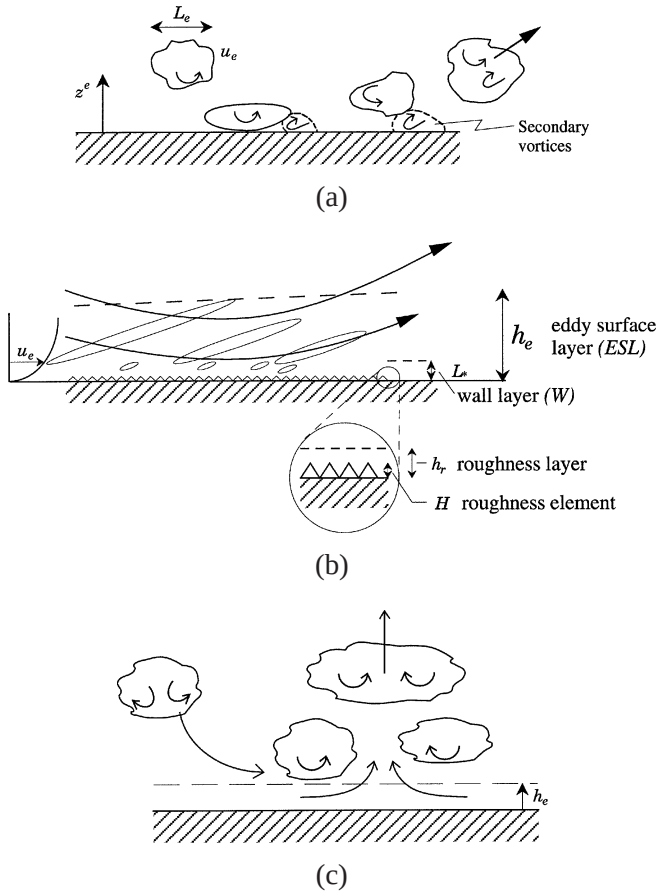

Figure 2. Effect of blocking – generation of anti-splats: (a) weak self-generation; (b) effect of blocking with shear – generation of secondary vorticity via surface instability; (c) eddy-eddy generation.

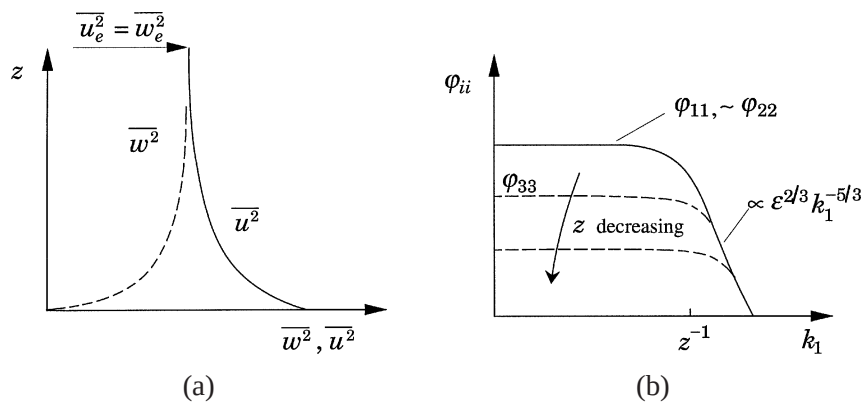

Figure 3. Effect of blocking alone in shear-free boundary layer (SFBL) on (a), variances and (b), spectra, $\varphi_{ii}(k_1)$ at a variable height. $\varphi_{11}(k_1 \to 0)$ and $\varphi_{22}(k_1 \to 0)$ increase as z decreases, $\varphi_{33}(k_1 \to 0)$ decreases as z decreases.

dissipation per unit mass, $\varepsilon(z)$, does not vary by more than a factor of 2 from its freestream value of $\varepsilon_E \approx \frac{u_E^3}{L_E}$ as z decreases towards the plate. This behaviour is quite different from that in sheared boundary layers where

ε increases towards the surface in proportion to z^{-1} until it reaches the very large value of order $\mathrm{Re}\,\varepsilon_E$ within the viscous sublayer.

Since the mean square vorticity, $\overline{\omega^2}$, in high Reynolds number turbulence is proportional to ε, this means that $\overline{\omega^2}$ is also approximately constant with height. Calculations for homogeneous (but not necessarily isotropic) freestream turbulence, having a full spectrum with an inertial subrange shows that, near the surface $h_s \ll z \ll L_E$, the variances of the parallel and normal velocities are:

$$\begin{aligned} \overline{u_s^2} &= \overline{u^2} + \overline{v^2} = 3\overline{u_E^2} - \alpha_s(\varepsilon z)^{2/3}, \\ \overline{w^2} &= \alpha_K(\varepsilon z)^{2/3}, \end{aligned} \tag{2}$$

where the dimensionless coefficients α_s and α_K are of the same order and simply related. Note how the smaller effects of blocking on smaller eddies means that the normal velocity increases more rapidly away from the wall than that of a single eddy – compare equation (1) with equation (2). For wave numbers of small eddies such that $k_1 > z^{-1}$, the wall has no effect, whereas for the larger scales, because they are blocked, the spectrum of the normal component has a constant value:

$$\varphi_{33} = \alpha_3 \varepsilon^{2/3} z^{5/3} \tag{3}$$

that matches the small scale spectra at $k_1 = z^{-1}$. This implies that the streamwise correlation length scale of the vertical fluctuations is given by:

$$L_{33}^{(1)} \sim z. \tag{4}$$

Note that for the parallel components, although their energy is changed, the form of their spectra is not because of potential velocity fluctuations. Thus:

$$\varphi_{11} = \varphi_{E_{11}} \quad (k_1 \to 0). \tag{5}$$

The correlation between the vertical eddy motions at different heights above the wall, $R_{33}(0, 0, r)$ (where $r = z/z'$, and where the 'reference' height z' is less than L_E) has a self-similar form when it is normalised on the variance at z', viz:

$$R_{33} = \frac{\overline{w(z)w(z')}}{\overline{w(z')^2}} = f(r). \tag{6}$$

Hunt et al. [20] showed how the form of $f(r)$ can be explained in terms of eddy analysis and leads to

$$R_{33} \approx r. \tag{7}$$

This is similar to the roller eddies concept of Townsend [3].

2.2.2. Surface effects

The inviscid blocking effect (i.e. $w = 0$ at $z = 0$) causes the normal component of the eddy velocity to be reduced to zero. Because of the no-slip condition at a rigid surface, the parallel component of velocity $u_s = \sqrt{\overline{u^2} + \overline{v^2}}$ must also decrease to zero at $z = 0$. However h_e is generally determined by the balance between the diffusion of 'secondary' vorticity from the surface ($\omega_2 = \frac{\partial u}{\partial z}, \omega_1 = -\frac{\partial v}{\partial z}$) and its advection parallel to the surface at a velocity u_s. If the Reynolds number of the eddy, $\mathrm{Re} = \frac{u_e L_e}{\nu}$ is 'large', then the surface layer thickness h_e is typically significantly less than L_e, being of order $L_e\,\mathrm{Re}^{-1/2}$. But if Re is even larger ($> 10^4$), then small

scale turbulence is generated in the surface layer below the eddy, and the structure changes, as shown by the statistical analysis in the next section.

Experiments on ring or line-pair vortices impacting onto rigid surfaces, such as those of Falco [11] or of well defined eddies within the turbulent flows, such as the eddy motion simulated by Perot and Moin [21], show that the surface shear layers do not just remain thin, but can grow to affect the whole eddy. This is because the secondary vorticity acts with the eddy's primary vorticity to lift the surface layer, as in a separating boundary layer: here, the thickening profile and the inflection profile amplifies the growth of disturbances, and leads to the sudden break up of the impacting vortices; see *figure 2*(*a*).

In a turbulent flow, laboratory observations and numerical simulations both show that the strongest upward motion or 'anti-splats' tend to be in the form of narrow plumes and to occur where the horizontal motion of one eddy collides with that of another one (Perot and Moin [21]). These ejections, which are driven by the interaction between the primary vorticity fields of the eddies, have an upward velocity of the order of u_e and are generally stronger than those caused by the interaction of an isolated vortex with its secondary vorticity which is mainly distributed along the surface, see *figure 2*(*c*).

The structure of the surface layer in which the tangential components for all wave numbers tend to zero as $z \to 0$, is dominated by the vorticity generated at the wall by the large scale eddies, and, as we shall see, diffused by viscosity or, at high Reynolds number, by small scale turbulence. Then h_e is greater than the length scale of the newly generated eddies. The surface layer below each eddy is coherent and behaves like a local mean flow $\langle u \rangle$ with smaller-scale fluctuations u' around this 'mean'. A theoretical analysis based on this 'scale separation' (Schumann [22], Hunt [23]) shows that the surface layer has a double/triple structure. Typically $h_e \approx \frac{1}{5} L_e$, depending on how the scale separation is exactly defined.

Within the layer, the structure changes at a characteristic height, $L_* = \frac{|u_{*e}|^3}{\varepsilon_E} \approx \frac{|u_{*e}|^3 L_E}{u_E^3}$. This is defined by the local wall friction velocity, u_{*_e}, and by the rate of dissipation of energy in the freestream. For $z > L_*$, the transport of momentum leading to the slowing down of the large eddies or 'mean' velocity is controlled by the freestream turbulent eddies, although blocked by the wall. For $z < L_*$, the structure of the 'mean' flow and the turbulence are determined by the local value of u_{*_e}, so that typically, $u_e \approx \frac{|u_{*e}|}{\kappa} \ln(\frac{L_*}{z_0})$ (where z_0 is the roughness length for a rough surface), or is equal to the surface viscous layer thickness, $\frac{\nu}{u_*}$, if it is smooth. In the eddy, $\varepsilon_e \propto \frac{u_{*e}^3}{z}$. For a smooth surface, the small scale fluctuations only decrease to zero in the viscous sublayer when $z < 30\frac{\nu}{u_{*e}}$.

Thus the criterion for the surface layer to have an asymptotically high Re structure can now be quantified (for the first time). On a rough surface, to satisfy the condition $h_e \gg L_* \gg z_0$, it is necessary that:

$$L_e \gg z_0 \left[\ln\left(\frac{L_*}{z_0} \right) \right]^3 \tag{8}$$

and on a smooth surface, to satisfy the condition $h_e \gg L_* \gg \frac{10\nu}{u_{*e}}$:

$$\mathrm{Re} > 10 \left[\ln\left(\frac{L_* u_{*_e}}{\nu} \right) \right]^4 \approx 10^4 - 10^5. \tag{9}$$

This is satisfied in geophysical flows, but not in many engineering flows in which SFBL's exist.

2.3. Shear boundary layers

The following analysis is useful for engineering problems in which a complex turbulent flow enters a pipe or initiates a boundary layer along a wall, as well as in situations in which a high Reynolds number boundary layer is constructed artificially using generators (Counihan [24], Cook [25], Hunt and Fernholz [14]). Based on this approach, the results of the previous sections and studies of turbulence mechanisms, some novel concepts are developed here for the structure of the turbulent boundary layer, especially at very high Reynolds number.

2.3.1. Uniform shear over a rigid boundary layer

Consider a homogeneous middle $[M]$ layer of relatively weak turbulence with rms velocity u_e and integral scale L_e placed in a uniformly sheared mean flow $U(z)$ above a rigid plane at $z = 0$, where the mean profile is such that there is a finite mean velocity U_s just above the very thin surface layer $[S]$ of thickness h_s ($\ll L_e$), so that $U = (U_s + \beta z, 0, 0)$ where $z > h_s$. We assume that the thickness of the middle layer is much greater than L_e and that the external region $[E]$ can be ignored in the interaction between $[M]$ and $[S]$.

This idealised problem has been analysed by Lee and Hunt [26] as an initial value linear problem, using rapid distortion theory, in which the turbulence adjusts between its form in uniform shear when $\frac{z}{L_e} \gg 1$ to the highly distorted form near the wall as $\frac{z}{L_e} \to 0$ when both blocking and shear operate together; see *figure 4*. The calculations of the spectrum show that the eddy structure is similar to that in the absence of the wall (Hunt and Carruthers [27]), except that, for those scales greater than the distance z from the wall, the vertical component is blocked, just as in a SFBL.

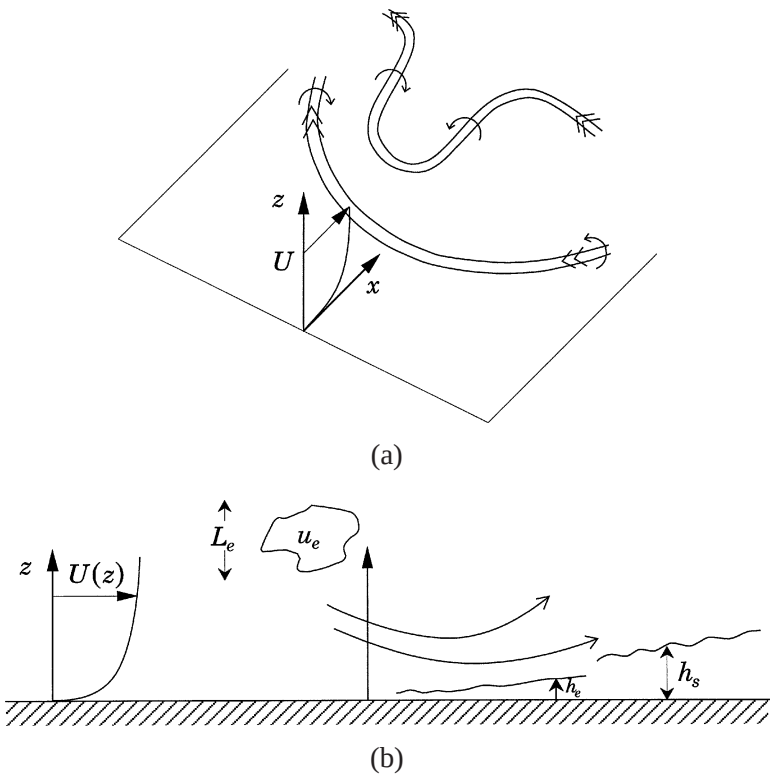

Figure 4. Effect of shear and blocking together: (a) reduced vortex bending near the surface reduces tangential components while splat increases them; (b) splat leads to generation of internal shear layer.

2.3.2. Length scales and the development of the mean velocity profile

The mean velocity profile in the surface layer is determined by a local dynamical balance. First consider an artificial boundary layer consisting of a shear layer above a rigid surface and created at $t = 0$. The blocking reduces $\overline{uw}$ to zero at the surface over a height of order L_e. Therefore $\frac{\partial^2}{\partial z^2}(-\overline{uw}) < 0$ and hence $\frac{\mathrm{d}}{\mathrm{d}t}(\frac{\partial U}{\partial z}) < 0$ so that the shear decreases and the boundary layer cannot sustain itself. However because of the surface eddy interactions, the shear stress near the surface is comparable to its value above the surface and therefore in general $\frac{\partial^2}{\partial z}(-\overline{uw}) \geqslant 0$. This is the key mechanism for sustaining high Reynolds number boundary layers.

However there are some significant differences as compared with SFBL's. Firstly, there is an increased tendency for the longitudinal vorticity and associated vertical velocity to induce 'streaks' in the streamwise velocity fluctuations; this is made clear in the spectra of $\varphi_{11}(k_2)$ which in the linear calculations has a noticeable peak at the streak spacing. (This peak is generally smeared out in fully non-linear calculations because the streaks undulate in the (x, y) plane.) Secondly, the wall affects the streamwise vortices generated by the shear; when they are in pairs or other grouping they move bodily up and down; those approaching the wall are affected by their image vortices and, by the kinematics of the process (see *figure 4*), are then spread out. Generally, as in SFBLs, these vortices meet other vortices near the surface and cause updrafts or ejections. Because of the different nature of the impinging vortices in a shear flow, the interactions and ejections are more effective in shear flows than in SFBL's.

2.3.3. Spectra

From these results and the concept of impinging and developing eddies in [S], the forms of the spectra of the horizontal and normal spectra can be derived, using statistical and scaling arguments. Their interpretation in terms of eddy structure is left to section 3. Consider the smallest eddies at each height, say $k_1 > k^*$, whose local fluctuating strains are larger (but not necessarily much larger, because of their shear sheltering properties – Hunt and Durbin [19]) than those of any large scale straining. As in many other inhomogeneous and anisotropic turbulent flows, the second-order moments and two-point spectra are isotropic and are determined by Kolmogorov's inertial range theory:

$$\varphi_{ii}(k_1) = \alpha_K \varepsilon^{2/3} k_1^{-5/3}, \tag{10}$$

where $\varepsilon \approx u_*^3/z$. Thus in the surface layer the inertial subrange extends to ever smaller scales as the surface is approached. Note that the effect of the mean shear $\partial U/\partial z$ is to make a small distortion of these eddies over a short time scale of $\varepsilon^{-1/3} k_1^{-2/3}$ so that, following Wyngaard and Cote [28] and Saddoughi and Veeravalli [29],

$$\varphi_{13}(k_1) = \alpha_\tau \frac{\partial U}{\partial z} \varepsilon^{1/3} k_1^{-7/3}. \tag{11}$$

Since the mean shear mainly determines the dissipation scale, it also determines the cut off wave number $k^* \approx (\frac{\partial U/\partial z}{\varepsilon^{1/3}})^{3/2}$. Note that in the surface layer, where $\partial U/\partial z \propto z^{-1}$, $k^* \propto z^{-1}$. This is the same result as for the SFBL, but because shear strain produces smaller scales, the value of $k^* z$ is larger here. Note that when $k < k^*$, the eddies at height z are then larger than the distance to the wall; the resulting distortion caused by the blocking considerably affects their dynamics as we shall see.

The largest scale motions in the middle layer [M] are those induced at its lower edge ($z \approx h_s$), so that for the horizontal component here,

$$\varphi_{11}(k_1 \to 0) \sim u_*^2 h_s. \tag{12}$$

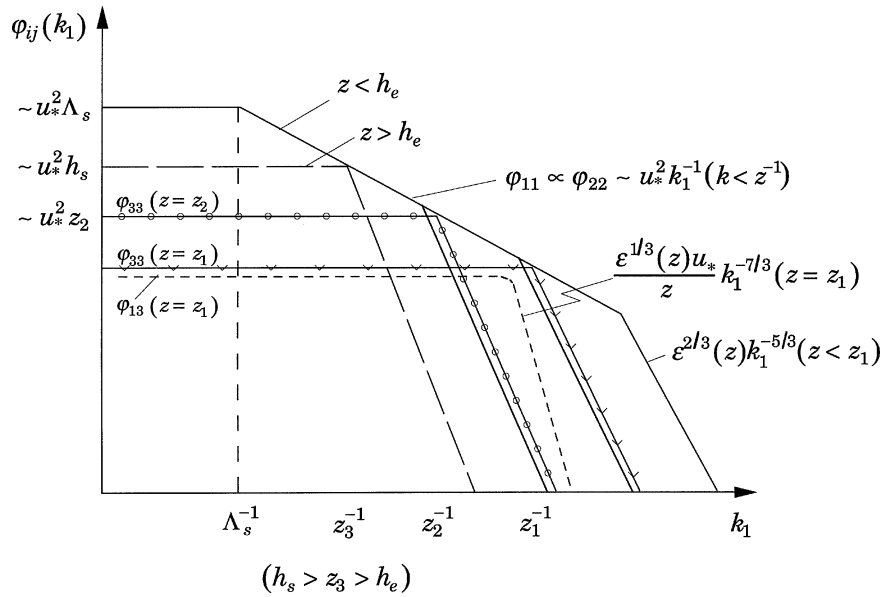

Figure 5. Representative one-dimensional spectra, $\varphi_{ij}(k_1)$ in the surface layer: showing how φ_{11} and φ_{22} (——— and — — —) change their structure between the surface layer $[S]$ and the eddy surface layer $[ESL]$ while φ_{13} (- - - - -) and φ_{33} (• • • • and ∨ ∨ ∨ ∨) do not. Note $z_1 < z_2 < h_e < z_3 < h_s$.

However, at very low wave numbers, a different spectral form is found in the eddy surface layer when

$$\varphi_{11}(k_1 \to 0) \sim u_*^2 \Lambda_s, \tag{13}$$

where a 'break point' occurs at $k_1 \approx \Lambda_s^{-1}$ and $\Lambda_s \approx \frac{hU}{u_*}$ for high Reynolds number boundary layers; see *figure 5*. This surface streamwise length scale is considerably longer than h.

In the intermediate range in which $h_s^{-1} \ll k_1 \ll \Lambda_s^{-1}$, where the eddies are larger than the distance to the surface, but independent of the larger-scale and three-dimensional dissipation-scale turbulence, scaling arguments indicate (Perry and Marušić [5], Perry and Abell [30,31]) that the spectra for the horizontal components is determined by u_* and k_1 only, so that

$$\varphi_{11} \propto \varphi_{22} \propto u_*^2 k^{-1}. \tag{14}$$

This follows from the fact that, over this scale range, there is a wide range of statistically independent and weakly interacting elongated structures, there being no single dominant eddy structure, such as a vortex filling the surface layer.

However the normal component is reduced by blocking, as in the SFBL. Hunt and Carlotti [32] show that in $[S]$ the form of the normal spectrum and the Reynolds shear stress co-spectrum in the inertial range are similar, viz:

$$\varphi_{33}(k) \sim \varepsilon^{2/3} k^{-5/3} \sim u_*^2 z, \tag{15}$$

and

$$\varphi_{13}(k < k^*) \sim \beta \varphi_{33} \sim u_*^2 z,$$

where β is a constant of order unity related to the mean non-dimensional shear (Townsend [3]). Integrating these expressions, it follows that the variances are given by:

$$\overline{u^2} \sim \overline{v^2} \sim u_*^2 \ln\left(\frac{\Lambda_s}{z}\right) \tag{16}$$

and

$$\overline{w^2} \sim u_*^2. \tag{17}$$

Note that this is not consistent with the simple attached eddy model proposed by Townsend ([3, p. 155]) or indeed, the forms proposed by Marušić et al. [33]. It follows that the streamwise integral scale for the horizontal component is:

$$L_{11}^{(1)} = \frac{\pi \varphi_{11}(k \to 0)}{\overline{u^2}} \approx \frac{\Lambda_s}{[\ln \frac{\Lambda_s}{z}]}. \tag{18}$$

Thus unlike the SFBL, $L_{11}^{(1)}$ decreases as $z \to 0$, and $L_{11}^{(1)} \ll \Lambda_s$, a result which is consistent with Counihan's [24] experimental data.

3. Observations and mechanisms of turbulent boundary layer structure

We now examine measurements and qualitative phenomena in atmospheric and laboratory boundary layers in order to elucidate the principal mechanisms and features of eddy structure at high Reynolds numbers $\mathrm{Re}_\tau > 10^4$ (equation (9)).

3.1. High Reynolds-number mechanisms

The origins of this 'top-down' model owe much to the flow visualization studies, especially Scorer's (private communication) whose photographs are reproduced in *figure 6*. Clearly visible on the surface of the water are 'cat's paws' (or 'splats') which are advected in the streamwise direction while splaying out in the spanwise direction. They form a staggered array on the surface of the water, and occasionally, adjacent cat's paws interact. *Figure 7* illustrates the model: a downdraft (or sweep) with vertical velocity, w_d, and height, z_d, moves down toward the surface creating a cat's paw. This leads to the generation of an inner shear layer of height, h_s, length, L_s, in the direction of the advected cat's paw, and, on either side of it, streamwise vortices are produced by blocking (cf. Kline et al. [34], or the 'pockets' of (Falco [11])). Brown and Thomas [35] also suggested the importance of the large scales in generating small-scale disturbances near the wall. Possible structures for the streamwise vortices are Townsend's [3] self-similar attached wall eddies of length L_s and height h_e ($h_R < z < h_e < h_s$). It is proposed that the eddy shear layer attached to an impinging structure grows until the two streamwise vortices (of opposite sign) interact to create an updraft (or ejection) with vertical velocity, w_u. The shear in $[S]$ leads to a generation of turbulence energy (and stress) and some of this energy is transported upwards back into $[M]$, even into the top of the outer layer.

The dynamics of eddies as they move between the wall and middle regions of the boundary layer have been considered previously by Kline et al. [34], Head and Bandyopadhyay [10] and Falco [11,12] with Re_τ in the range 100–1000. Typically, velocity fluctuations grow in $[S]$ leading to the transport of energy from these regions into $[M]$. *Figure 7*(*b*) shows the model at these lower Reynolds numbers where a downdraft is closely followed by a subsequent updraft, giving rise to an internal near-wall shear layer (Robinson [36]). Even though

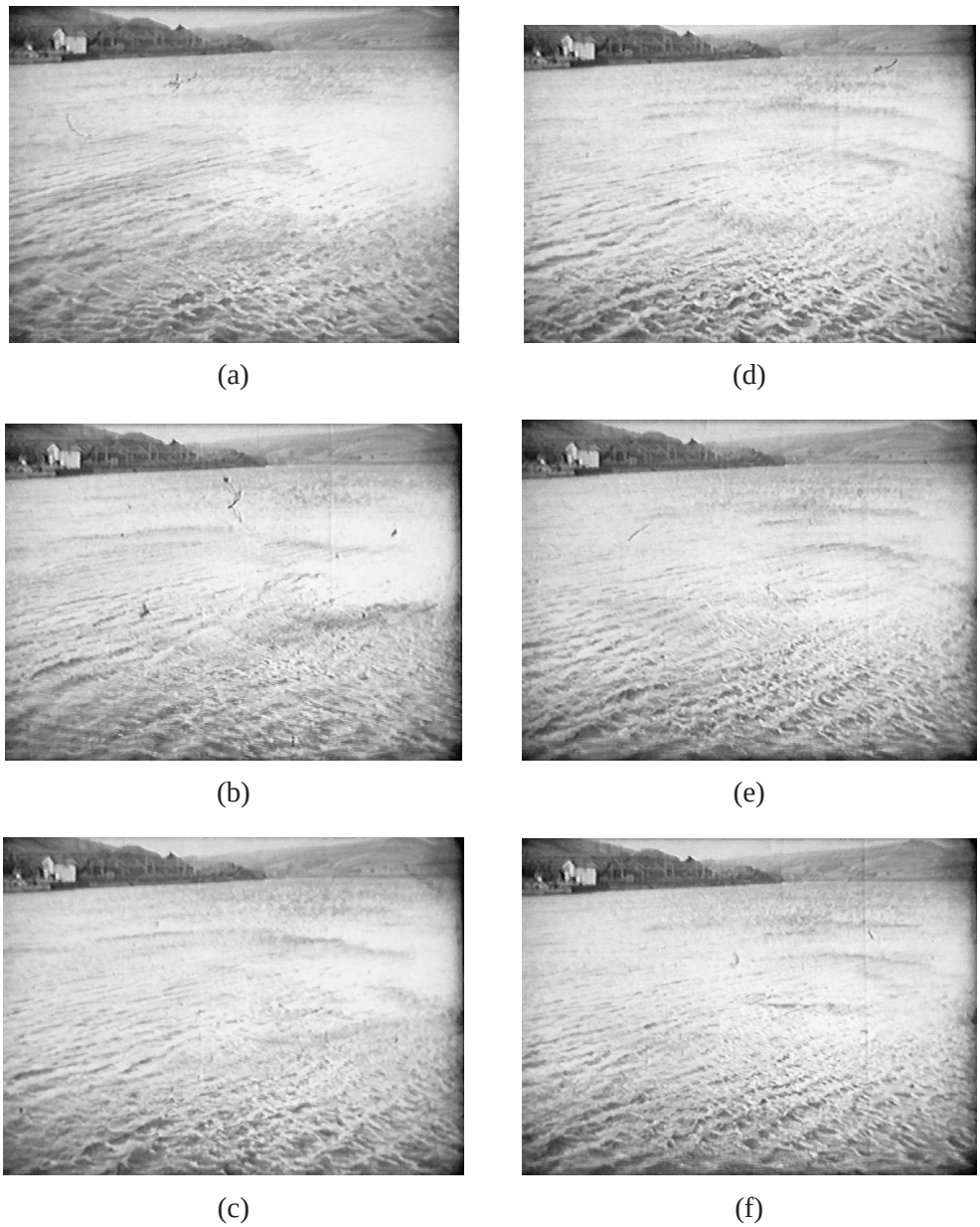

Figure 6. Photographs from Scorer (private communication): sequence (a) to (f), $t = 0$, 0.3, 0.8, 1.2, 1.6 and 1.9 s respectively.

the fundamental mechanism involves streamwise vortices, spanwise vorticity is also generated in the wall shear layer and this is the component most often measured by experimentalists. Single-probe results can give the false impression that updrafts follow downdrafts in the streamwise direction whereas Robinson shows that this is hardly ever the case and that ejections and sweeps are also separated in the spanwise direction occurring around either streamwise vortices or arch vortices. Morrison and Bradshaw [37] show that the streamwise wall-pressure gradient beneath a sweep is large and positive closely followed by a region of high shear (a near-wall shear layer). More or less immediately, this initiates an ejection beneath which the streamwise wall-pressure

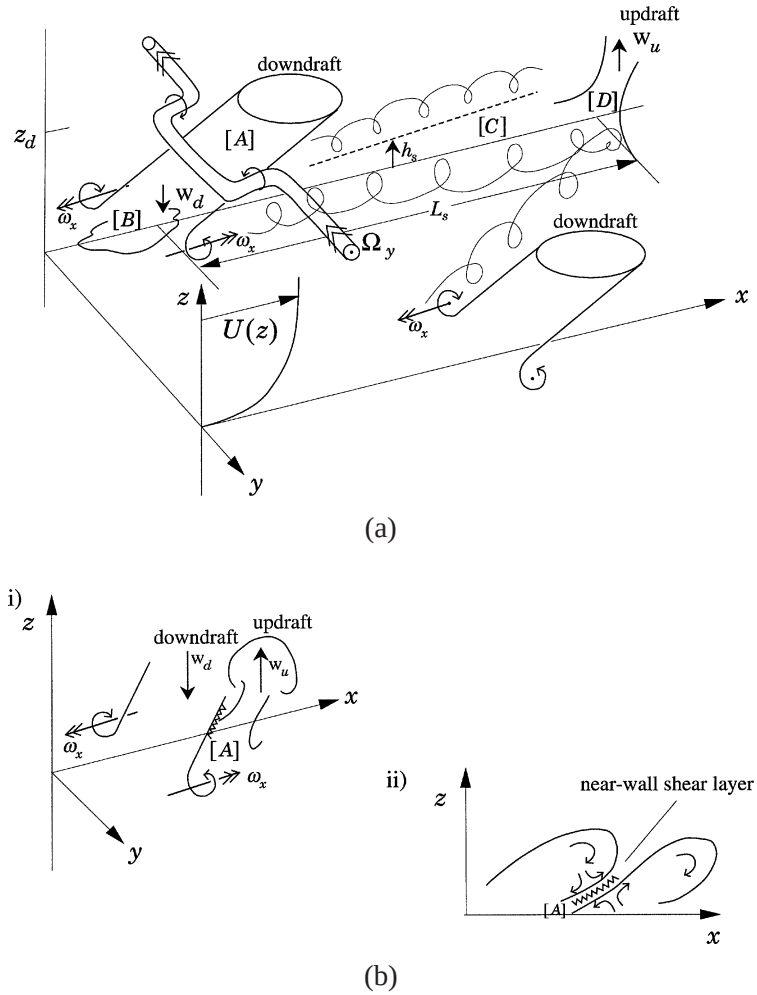

Figure 7. Schematic of model: (a) high Reynolds number: [*A*], downdraft with streamwise vorticity produced by self-induction; [*B*], 'cat's paw' and generation of streamwise vortices; [*C*], eddy shear layer; [*D*], updraft via interaction of adjacent vortices. (b) Low-to-moderate Reynolds number; [*A*], internal shear layer (microfront). Velocity vectors in (ii) relative to large-scale convection velocity.

gradient is now negative. Mahrt and Howell [38] find similar behaviour in the atmospheric surface layer in which 'microfronts' are taken as regions of concentrated shear at the leading edge of a downdraft.

The proposed mechanism differs from those of recent DNS studies (e.g. Jiménez and Pinelli [39] and Schoppa and Hussain [13]) which suggest that the motion in [*S*] is generated by the viscous-inertial instabilities in the wall layer: in these studies, ejections are 'bottom-up' events. Holmes et al. [2] have suggested that these instabilities and growing fluctuations in [*S*] have a weak, but significant interaction with large pressure fluctuations generated in [*M*].

3.2. Observations

Figure 6 contains several features. The first of these are the cat's paws, sharply defined, isolated patches of capillary ripples on the surface of a reservoir (also seen on crop canopies or grass prairies) that move with the mean velocity equivalent to the wind speed a few metres above the surface. They are visible as light or dark

patches depending on the orientation of the observer to the sun and where the surrounding surface is smooth. In the atmospheric boundary layer ($h \approx 500$ m^{-1} Km), the scale of the cat's paws, is typically 5–10 m. They are initiated quite rapidly (≈ 1 sec) a period comparable to the time it takes for one to pass the observer. As they move in approximately the same direction as that of the mean velocity, they tend to widen steadily at an angle of about 10°, and lengthen slightly in the direction of flow. On an otherwise still ocean surface, cat's paws can be observed to travel for about 500 m^{-1} Km. Their relative spanwise positions vary so that sometimes they form either a staggered array while at other times they lie adjacent to one another.

The second observation is that of streaks of dust sand or snow over very flat surfaces of about 5–10 cm width and 10–20 m length. They lie parallel to the wind direction, the particles appear to be transported transversely and then lifted up. The spanwise undulation is of quite a long time scale (≈ 1 s) over distances of the order of their length. The speed of the particles varies with the wind speed suggesting that they persist as gusts pass over them. It is noticeable that smoke released above the ground, although wafting up and down and dispersing is not observed to follow any spiral pattern. These observations are consistent with those of Klewicki et al. [40].

The third observation is related to the influence of $[S]$ on the eddying motion in $[M]$. In the atmosphere, it is noticeable that smoke from a source near the ground tends to travel along the ground for 100–300 m in a layer of about 10 m thickness before the whole layer rises upwards in a short distance of 10–20 m, the smoke subsequently dispersing. A fourth observation can be made on the surface of rivers (typically of depth 5 m) where bulges of 1–2 m are caused by impinging eddies that have risen from the bottom.

These observations differ from those at low Reynolds number, particularly by the sharp intermittency and irregularity of the first, second and fourth. There are other phenomena, which are quite similar at low Reynolds number such as the behaviour of clouds of surface material being ejected upwards and distorted by the shear of the mean velocity profile. Real-time measurements of the velocity fluctuations in the atmospheric boundary layer do not show the same regular patterns as observed in low Reynolds-number flows.

3.3. Comparison of theory and statistical measurements

There are some key statistics that discriminate between different mechanisms at high and low Reynolds numbers. It is also useful to compare the results for zero freestream turbulence with those disturbed by high levels of freestream turbulence.

3.3.1. Mean profiles

For $\mathrm{Re}_\tau > 10^4$, the mean velocity profiles of boundary layers on smooth or rough walls in moderate pressure gradient are self-similar although their logarithmic form as Reynolds number and roughness vary are still controversial. Except in the roughness/viscous sublayer, the profiles of mean velocity and higher-order statistics are only affected by the average effects of motions in the viscous sublayer and over the roughness surface elements. The velocity fluctuations between the roughness elements are of order u_* between the elements, but increases rapidly when $z \geqslant z_0$. The interaction of the eddy motion between the roughness flow below the elements and the turbulence above them decreases rapidly across the shear layer. Shear sheltering (Hunt and Durbin [19]) across the inflection point is the chief mechanism for this de-correlation and this is why there are few large-scale gusts within an urban or natural canopy. Over a flat surface, the mean viscous stresses exceed the turbulent stresses for $z/h_R < 1$.

Similarly, there is a reduced penetration of the small-scale motion from the surface layer into the viscous sublayer on a smooth surface as shown by the weak correlation between the surface shear stress and the velocity at $z \approx h_R$. This is caused at high Reynolds numbers by the shear-sheltering mechanism. Therefore the viscous diffusion of vorticity from the surface up to height h_R is greater than $U(h_R)\nu/u_*^2$, so that, in practice,

$h_R u_*/\nu \approx 30$. Above the roughness sublayer, the gradient of the mean velocity profile over rough and smooth surfaces is approximately proportional to $\frac{u_*}{(z-d)}$ for $h_R < z < h_s$ where d is the displacement height.

Most the data show that κ is approximately constant whether for rough or smooth surfaces. The mean velocity profile in the surface layer is observed to have the form over rough surfaces:

$$U(z) = \frac{u_*}{\kappa} \ln\left(\frac{z-d}{z_0}\right) \tag{19}$$

for $h_s > z - d > z_0$, and over smooth surfaces:

$$U(z) = \frac{u_*}{\kappa} \ln\left(\frac{z}{\nu/u_*}\right) + C \tag{20}$$

for $h_s > z > h_R$. Note that as the Reynolds number decreases, $h_R u_*/\nu$ increases and the depth of the surface log layer, h_S (typically $0.2h$), decreases.

3.3.2. Attached and detached eddies

Using conditionally sampled data based on the uw product at moderate Reynolds numbers, Morrison et al. [8] showed that updrafts (ejections) of uw_2-quadrant motion reach the outer layer and are correlated with the wall shear stress, which is consistent with Townsend's attached wall eddy. Significantly though, they also showed that this correlation decreases significantly once the ejection reaches the middle layer [M] where the correlation length scale reduces to about one half of its maximum value occurring at the outer edge of the inner layer. These eddies are 'detached' from the surface and are evident in the numerical simulations analysed by Fung et al. [41]. Both Robinson [36] and Kim and Adrian [42] show that the surface layer [S] is densely populated with near-wall shear layers (contour surfaces of $|\omega|$ that are 30 to 60 viscous units wide and several hundred viscous units long), which in some instances, are lifted so that the head of the vortex rolls up and separates from the shear layer. Typically, this occurs near the outer edge of [S] and, if this occurs at much higher Reynolds numbers, this is one of the mechanisms for the detached eddies that are quite unconnected to the wall. It also provides a physical justification for the distinction between an inner and outer layer – i.e. the inner layer largely comprises attached wall eddies (quasi-streamwise vortices) while the outer layer consists mostly of detached eddies. Indeed, when these eddies impinge on the wall, they have a very significant effect. Support for the distinction between attached and detached eddies comes from the work of Perry and Marušić [5] and Marušić and Perry [43]. Zagarola and Smits [44] have suggested an outer velocity scale for pipe flow based on the velocity deficit. See also Katul and Vidakovic [45].

3.3.3. Statistical measurements

The combined effects of mean shear and blocking can be estimated using linear rapid distortion theory (Lee and Hunt [26]). Consider the integral scale $L_{33}^{(1)}$ of the normal velocity component in the streamwise direction, approximately equal to the dissipation length scale, L_ε in shear-free and sheared boundary layers. This is affected by the mean shear and blocking so that the effect of producing the small scales dominates, i.e.

$$\left(L_{33}^{(1)}\right)^{-1} \approx L_\varepsilon^{-1} \approx \frac{A_B}{z} + A_S \frac{\partial U/\partial z}{\sqrt{\overline{w^2}}}, \tag{21}$$

where A_B and A_S are both of order one (Hunt et al. [20]). This relation shows that both effects are comparable in the neutrally-stratified non-accelerating surface layer.

The self-similar form of the two-point correlation, $R_{33} \approx r$ (equation (7)), should be found in very high Reynolds number boundary layers. The measurements of R_{33} at the Boulder Atmospheric Observatory agreed this result both for neutral conditions (with shear) and convecting conditions without mean shear. However, numerical simulations at lower Reynolds numbers show that R_{33} is less than the inviscid value although it still has a roughly self-similar form. The extra contribution of the blocking effect at very high Reynolds numbers is apparent in the measurements of $\overline{w^2}$ in the atmospheric boundary layer. At moderate Reynolds numbers, it decreases from its maximum value at the top of the roughness layer but Högström [46] shows that it increases with z at the bottom of the surface layer ($z/h < 0.03$). This result is consistent with large-scale eddies at the top of the surface layer impinging onto the ground and adding to the small-scale turbulence produced near the surface. Following the argument of Hunt [16], it can be expected that

$$\overline{w^2} = \lambda_B u_*^2 \left(\frac{z}{h_s}\right)^{2/3} + \lambda_S u_*^2. \tag{22}$$

Replotting the data in this form shows that λ_B and λ_S are constants of order one (Högström, private communication).

Figures 8 and *9* shows velocity spectra from Hoxey and Richards [47] and Richards et al. [48]. In *figure 8*, they are re-scaled in the form $\frac{k_1 z \varphi_{ii}(k_1 z)}{-(\overline{uw})}$, using wall scales $(-\overline{uw})^{1/2}$ and z such that the integral of the spectrum yields the variance (or covariance) normalised by $\overline{uw}$. The streamwise wave number is defined by $k_1 = \frac{2\pi f}{U}$. Pre-multiplication by $k_1 z$ ensures that both the ordinate and the area beneath the spectrum are proportional to the energy. In this form, the spectra in the inertial subrange should collapse on

$$\frac{k_1 z \varphi_{ii}(k_1 z)}{-(\overline{uw})} = \frac{\alpha_K}{\kappa^{2/3}} (k_1 z)^{-2/3}, \tag{23}$$

the expected form deduced from the local equilibrium approximation. We take the constant as $\alpha_K = 0.5$ for φ_{11} and $\frac{4}{3}\alpha_K$ for φ_{22} and φ_{33}. *Figures 8*(*a*) and *8*(*b*) show that equation (23) is an accurate estimate for the horizontal velocity components, but *figure 8*(*c*) shows that it is less accurate in the case of φ_{33}. The ratio $-\overline{uw}/u_*^2$ is close to unity except at the lowest height which may well be influenced by surface roughness such that there is significant transport of energy towards the surface to match the increased dissipation there. Thus $-\overline{uw} \neq u_*^2$, justifying the choice of wall scaling (even though strictly this invalidates the deduction of a k_1^{-1} range by dimensional arguments). In *figure 9*, the same data are also plotted as $\frac{k_1 h \varphi_{ii}(k_1 h)}{u_*^2}$ using outer scaling u_* and h (≈ 500 m). Although the data suffer from limited time resolution (especially near the surface) and from low-frequency unsteadiness that is invariably present in data of the atmospheric boundary layer, they provide a valuable insight into the eddy structure near the surface.

In the range $0.01 < k_1 z < 1$, $\varphi_{11}(k_1 z)$ and $\varphi_{22}(k_1 z)$ collapse and indicate a region in which $\varphi \propto k_1^{-1}$ (a horizontal line with the present scaling). The extent of this region decreases with increasing height owing to the decreasing effects of shear-sheltering. Although the ambiguities of the low frequency behaviour also make deductions difficult in this range, it is clear that the collapse of either φ_{11} or φ_{22} with outer scaling (*figures 9*(*a*) and *9*(*b*)) is less successful. At the two larger heights, a k_1^{-1} range is apparent.

At very low wave numbers, the break in the spectrum occurs at a wave number φ_{11} ($k_1 \to 0$), corresponding to a very long length scale. The analysis of section 2.3.3 suggests that φ_{11} ($k_1 \to 0$) is of order $u_*^2 \Lambda_s$. Estimates of $\frac{\varphi_{11}}{u_*^2 h}$ at $k_1 h = 0.1$ suggest that $\frac{\Lambda_s}{h} \approx 0.2$ at the lowest height, but increases up to 4 at 10 m. Similarly, taking the 'break point', $k_1 \sim \Lambda_s^{-1}$, at which $\frac{\varphi_{11}}{u_*^2 h}$ in *figure 9*(*a*) enters the $\varphi \propto k_1^{-1}$ range as $k_1 h \approx 2$, gives $\frac{\Lambda_s}{h} = \frac{2\pi}{k_1 h} \approx 3$. Other meteorological data (Davenport [49], Colmer [50], Lauren et al. [51], Fuehrer and Friehe [52]) all confirm

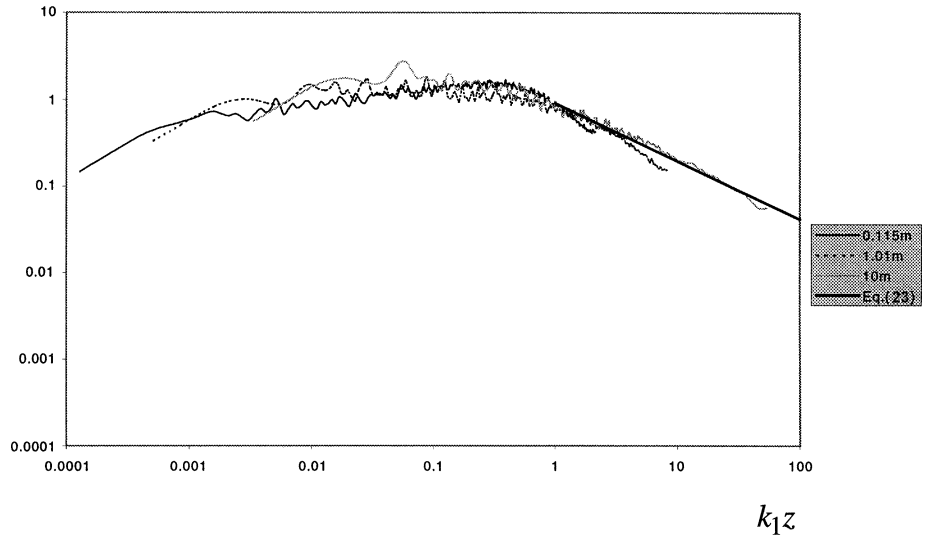

(a)

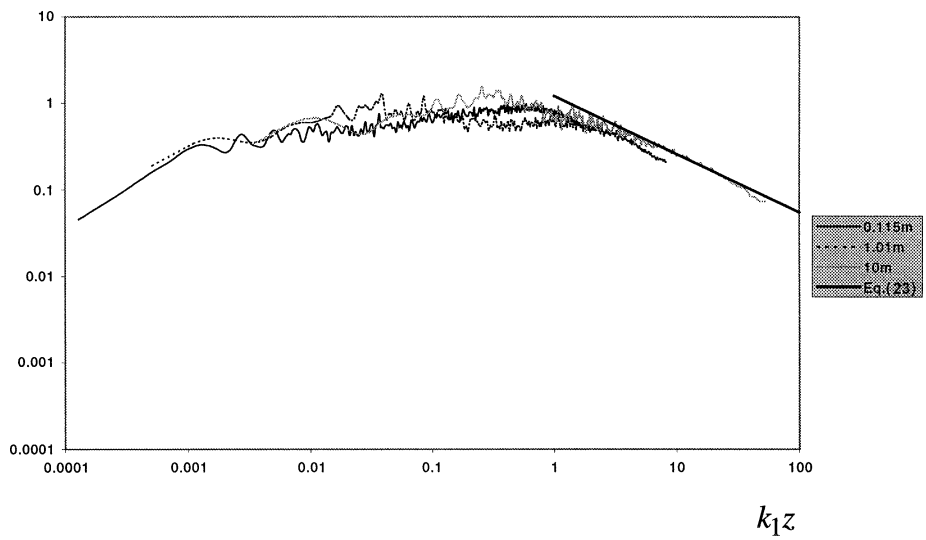

(b)

Figure 8. Scaled spectra from Hoxey (private communication), $\frac{k_1z\varphi_{ii}(k_1z)}{-(\overline{uw})}$ *vs.* k_1z: (a), φ_{11}; (b), φ_{22}.

this estimate. However, there is an inconsistency between the present results and those of Kader and Yaglom [4] which do not show this 'break point' in the φ_{11} spectrum. However, Kader and Yaglom's spectra only extend down to $k_1z \approx 0.01$.

The power spectrum for the vertical component and the uw cross spectrum (together with the theory of section 2.3.3) are quite different. At low wave numbers, the concept of blocking of the self-similar surface-normal component implies that $\frac{k_1z\varphi_{33}(k_1z)}{-(\overline{uw})} \propto k_1z$ and the spectra at these wave numbers should collapse. It is clear in *figures 8*(*c*) and *8*(*d*) that they do and that at low wave numbers, the wave number at which blocking occurs is inversely proportional to z. At $k_1z \approx 1$, the eddies become smaller in size than z so that blocking is

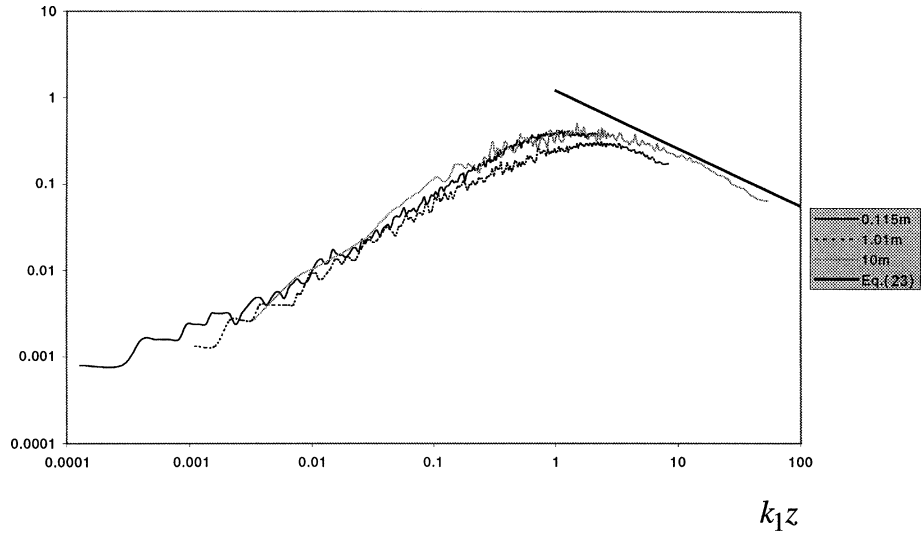

(c)

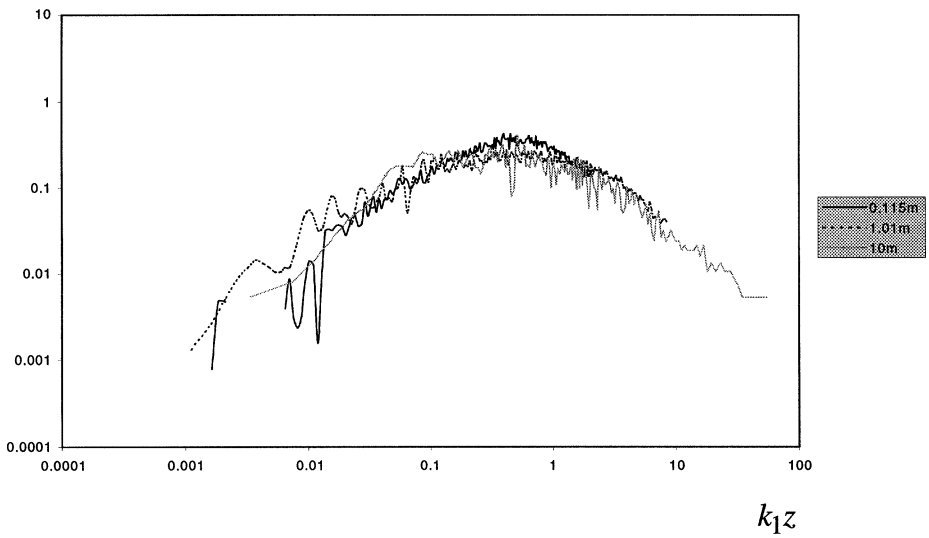

(d)

Figure 8. (Continued.) (c), φ_{33}; (d), φ_{13}. Symbols: ———, 0.115 m; - - - - -, 1.01 m; · · · · · · · · ·, 10 m.

no longer effective and they tend to become more isotropic. Thus at all three heights, the φ_{33} spectra reach a plateau prior to the $-2/3$ slope of the inertial subrange. Similar arguments apply to the φ_{13} co-spectra (*figure 8*(*d*)) in which self-similar parts of the w velocity field correlate with those parts of the u velocity field. Furthermore, at $k_1z \approx 1$, φ_{13} is a maximum indicating that the lower wave-number end of the inertial subrange has significant shear stress (Saddoughi and Veeravalli [29], Morrison et al. [8]). For $0.1 < k_1z < 1$, approximately, it is possible that $\varphi_{13} \propto k_1^{-1}$ in between the self-similar range, and the upper limit to the blocking range, $k_1 \approx z^{-1}$, as Jiménez [53] suggests. Kader and Yaglom [4], Wyngaard and Cote [28] and Saddoughi and Veeravalli [29] all show that φ_{13} decreases as $k_1^{-7/3}$in the inertial subrange.

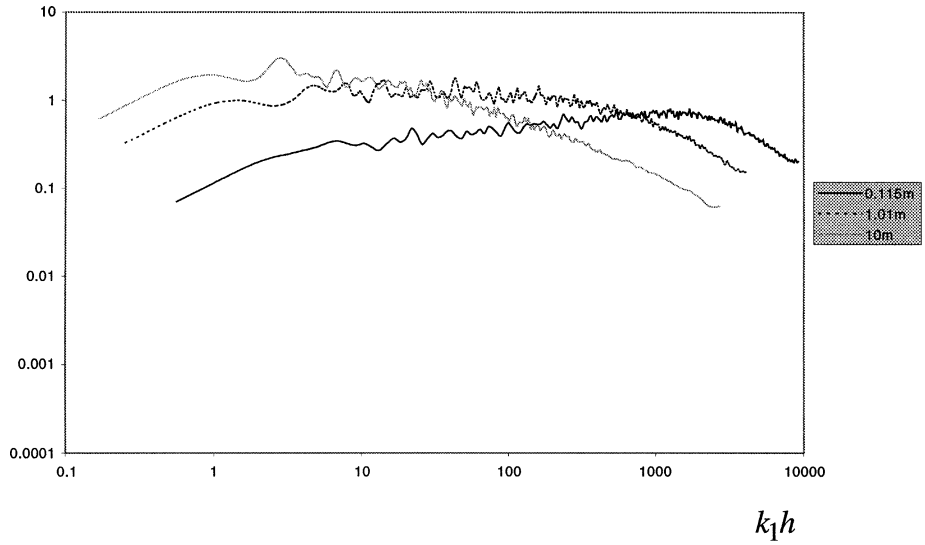

(a)

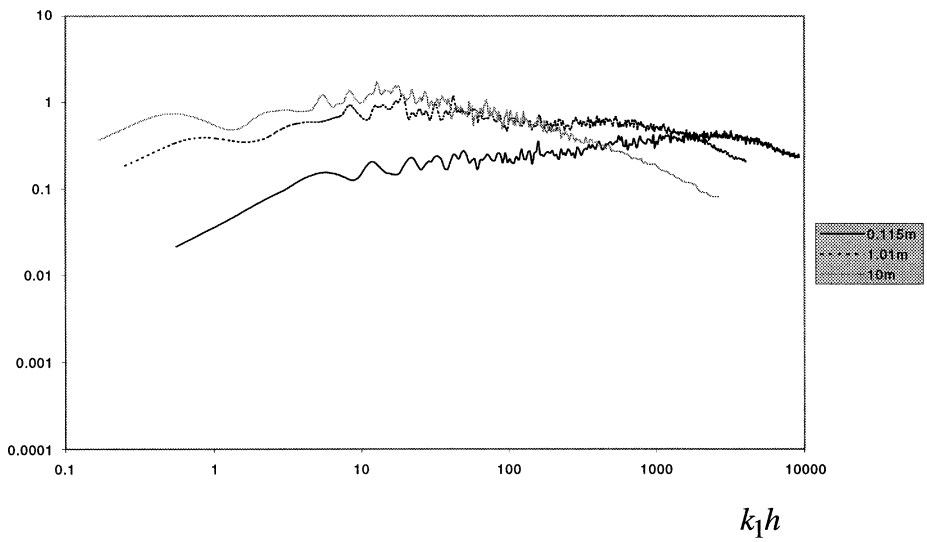

(b)

Figure 9. Spectra (same data) scaled as $\frac{k_1 h \varphi_{ii}(k_1 h)}{u_*^2}$ *vs.* $k_1 h$: sequence and symbols as in *figure 8.*

In the laboratory, very high Reynolds-number data are becoming available from the 'Superpipe' data at Princeton (Zagarola and Smits [44]). Williams [54] has provided measurements of φ_{11} up to Reynolds number based on pipe diameter, $\mathrm{Re}_D = 4 \times 10^6$ in both the outer part of the log region as well as the outer layer. In these preliminary data, the inertial subrange slope is readily apparent (on log-log axes), even at the lowest $\mathrm{Re}_D = 3.5 \times 10^4$. A k_1^{-1} range is also apparent and, in conformity with previous arguments, it is most extensive at the highest Re_D at the position closest to the wall $(0.4D)$ for $1 \leqslant k_1 D \leqslant 10$ approximately, in agreement with the data of *figure 9*. Generally, it extends up to $k_1 z \approx 1$, obviously where the eddy size $\propto z$. Kim and Adrian [42] have also made measurements of φ_{11} in a pipe up to $\mathrm{Re}_D = 1.15 \times 10^5$. Moreover, the data are

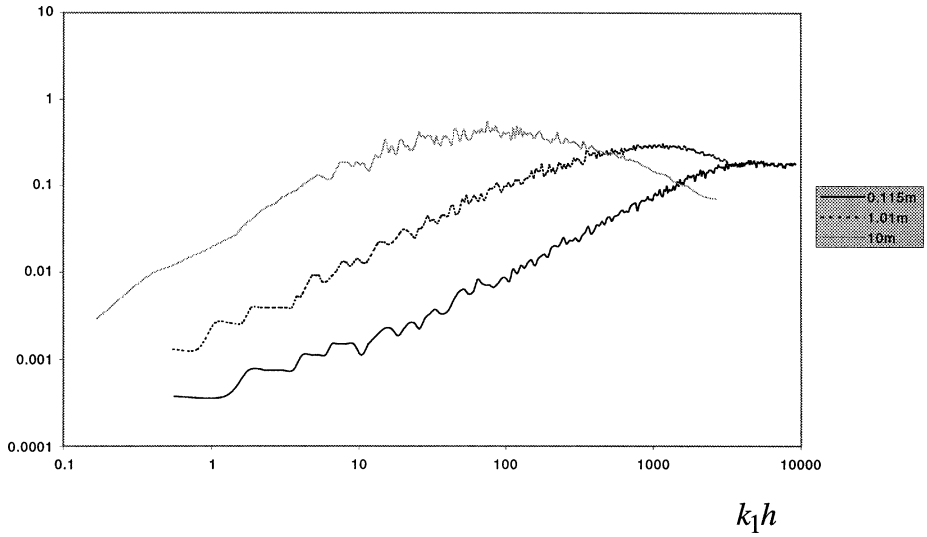

(c)

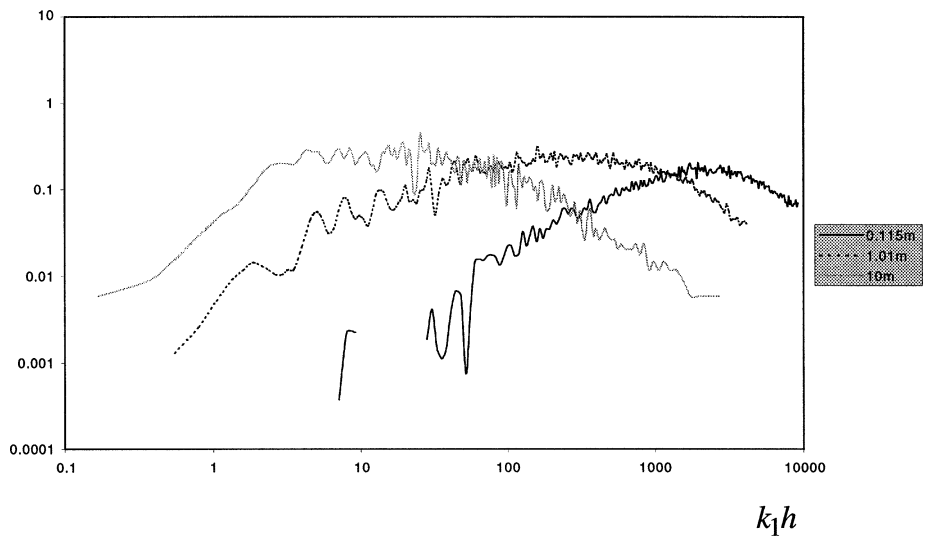

(d)

Figure 9. (Continued.)

presented in the same form as that of *figures 8* and *9*. This presentation removes ambiguities concerned with fitting spectral slopes to smoothly varying spectra. The spectra confirm the existence of the k_1^{-1} range up to a height of about $0.4D$, and, in addition to the large eddies of scale D, they measured Λ_s and confirmed the presence of 'very large scale motions (VLSMs)' with largest wavelengths of about 10 to 15 pipe radii, R, in the outer part of the log region. VSLMs comprising 'packets of hairpin eddies' (of scale Λ_s) therefore make the k_1^{-1} range more plausible. They found that Λ_s increases quickly near the wall to a maximum of about $15R$ at $z/R = 0.2$ (in our notation). The 'Superpipe' data suggest $\Lambda_s \approx 18R$, at $\mathrm{Re}_D = 3.5 \times 10^5$ with a possible increase to about $40R$ at $\mathrm{Re}_D = 4 \times 10^6$. This is significantly different from that observed in the atmosphere (Davenport [49], Lauren et al. [51] and Hoxey and Richards [47]) where Λ_s/h is about 3 to 5 only. The data

of *figure 9* show modest increases in Λ_s/h with height, but are inconclusive as to whether it increases further away from the surface. The pipe result is consistent with eddies in the wall region being strained and therefore less disrupted by large-scale energetic eddies from the outer region. Jiménez [53] has identified very long wavelengths in DNS data of turbulent channel flow. The importance of VLSMs can not be over-emphasized. In particular, their existence implies that simulations should have spatial domains of order $50h$ (that is 10 VSLM turn-over times) rather than $10h$ currently used!

4. Discussion

We have proposed here an outline structure for the mean flow and large scale turbulence in neutrally stratified turbulent boundary layers at very high Reynolds number over flat surfaces. This is a modification and extension of earlier proposals, notably those of Townsend, Perry and Adrian. The mechanisms are based on idealised studies of turbulent flows distorted by mean shear and by the effects of rigid boundaries. Based on qualitative observations of eddies in the atmospheric boundary layer, and from numerical simulations of idealised flows, we have considered some typical forms of the large scale eddy structures, and after some order of magnitude analysis showed that these only occur at very high Re_τ ($> 10^4$) or over rough surfaces.

The dominant mechanism is that large scale eddies in the middle layer impinge at the wall and as they move along with the mean flow, they are decelerated, while generating rapidly increasing shear stresses within internal shear layers. On impingement, the vortical eddies develop longitudinal structures, with a characteristic spectral form, and when they interact with others they are ejected upwards, even as far as the other side of the boundary layer or channel flow. This process maintains the Reynolds shear stresses and the mean velocity gradient. It also leads to the generation of small-scale turbulence and some upscale transfer of energy. This 'top-down', integrated picture differs from the 'bottom-up' instability – surface interaction mechanisms proposed by most authors. It appears that that the latter is valid for $\mathrm{Re}_\tau < 10^4$ but above that, there is a steady trend to the 'top-down' structure. These concepts may shed light on the earlier analysis of the inner and outer interactions in terms of active and inactive motions (Townsend [3,6], Bradshaw [7], Morrison et al. [8]).

The transition between the two descriptions is consistent with the distinction between attached wall eddies and detached eddies (Morrison et al. [8], Perry and Marušić [5]). The influence of the latter increases with Re_τ but is smaller in channel and pipe flows, thus enabling the formation of VLSM's of scales greater than $5R$. The existence of VLSM's extends the k_1^{-1} region in the spectra of the tangential velocity components, an equivalent physical-space description being the effect of shear-sheltering in de-correlating the inactive motion (dependent on both *h and z*) from the active motion (dependent on z only). The influence of attached eddies also recedes as the wall-normal distance increases – Kim and Adrian [42] show that the wavelength of VLSM's drops off quickly at heights greater than about $0.4R$. This 'top-down' view (together with the concept of shear-sheltering) could be used to explain the Reynolds-number dependence of even the wall-normal velocity component of near-wall motion (Fernholz and Finley [55]). While it does not explain the persistence of the non-dimensional streak spacing ($\approx 100\frac{\nu}{u_*}$) at very high Reynolds numbers, it is perhaps consistent with this estimate which is certainly greater than the height below which models of 'bottom-up' instabilities are confined in simulations.

An important practical consequence of the model is that, as the Reynolds number increases, since the velocity becomes more a spatially random distribution of algebraically growing disturbances, turbulent boundary layers are less likely to be controllable in real time, than as appears to be possible at low Reynolds number, when the natural, exponentially growing instability modes near the surface can be suppressed. However there are certainly other ways in which their structure is sensitive to disturbances, such as that of aerodynamic flows to changes in surface roughness and external pressure gradients. In the model proposed here, the hypotheses

for eddy structure have so far only been tested quantitatively against atmospheric data. One hopes that in future new high-Reynolds-number facilities will enable these to be tested more precisely in laboratory flows.

Acknowledgements

We are very grateful for highly instructive conversations with many colleagues, especially R.P. Hoxey, F. Hussain, J. Jiménez, R.S. Scorer, P. Bradshaw, N.D. Sandham, P. Moin, D.J. Thomson, P.J. Mason, P. Bougeault, J. Magnaudet, P.A. Durbin, X. Wu, R.G. Jacobs, F.T.M. Nieuwstadt, R. Uitenbogaard, A.E. Perry and U. Högström.

This paper was written during the Isaac Newton Institute programme on Turbulence in 1999. We are very grateful to the organisers and sponsors co-ordinated by the Royal Academy of Engineering for the opportunity to have participated.

References

[1] Scorer R.S., Problems in atmospheric stratification, in: Wind-tunnel simulation of the atmospheric boundary layer: a report on Euromech 50, 1975; see Hunt and Fernholz [14].
[2] Holmes P., Lumley J.L., Berkooz G., Turbulence, Coherent Structures, Dynamical Systems and Symmetry, Cambridge University Press, 1996.
[3] Townsend A.A., The Structure of Turbulent Shear Flow, 2nd edn., Cambridge University Press, 1976.
[4] Kader B.A., Yaglom A.M., Spectra and correlation functions of surface layer atmospheric turbulence in unstable thermal stratification, in: Métais O., Lesieur M. (Eds.), Turbulence and Coherent Structures, Kluwer Academic Publishers, 1991, pp. 387–412.
[5] Perry A.E., Marušić I., A wall-wake model for the turbulence structure of boundary layers. Part 1. Extension of the attached eddy hypothesis, J. Fluid Mech. 298 (1995) 361–388.
[6] Townsend A.A., Equilibrium layers and wall turbulence, J. Fluid Mech. 11 (1961) 97–120.
[7] Bradshaw P., 'Inactive' motion and pressure fluctuations in turbulent boundary layers, J. Fluid Mech. 30 (1967) 241–258.
[8] Morrison J.F., Subramanian C.S., Bradshaw P., Bursts and the law of the wall in turbulent boundary layers, J. Fluid Mech. 241 (1992) 75–108.
[9] Barenblatt G.I., Chorin A.J., Scaling laws and vanishing viscosity limits for wall-bounded shear flows and for local structure in developed turbulence, Comm. Pure Appl. Math. 50 (1997) 381–398.
[10] Head M.R., Bandyopadhyay P., New aspects of turbulent boundary-layer structure, J. Fluid Mech. 107 (1981) 297–338.
[11] Falco R.E., Structural aspects of turbulence in boundary layer flows, in: Patterson G.K., Zakin J.L. (Eds.), Turbulence in Liquids, University of Missouri-Rolla, 1980, pp. 1–14.
[12] Falco R.E., A coherent structure model of the turbulent boundary layer and its ability to predict Reynolds number dependence, Philos. T. Roy. Soc. A 336 (1991) 103–129.
[13] Schoppa W., Hussain F., Genesis and dynamics of coherent structures in near-wall turbulence: a new look, in: Panton R.L. (Ed.), Self-Sustaining Mechanisms of Wall Turbulence Computational Mechanics Publications, Southampton, UK and Boston, USA, 1997.
[14] Hunt J.C.R., Fernholz H.-H., Wind-tunnel simulation of the atmospheric boundary layer: a report of Euromech 50, J. Fluid Mech. 70 (1975) 543–559.
[15] Panton R.L. Self-Sustaining Mechanisms of Wall Turbulence, Computational Mechanics Publications, Southampton, UK and Boston, USA, 1997.
[16] Hunt J.C.R., Turbulence structure in thermal convection and shear-free boundary layers, J. Fluid Mech. 138 (1984) 161–184.
[17] Wood D.H., Bradshaw P., A turbulent mixing layer constrained by a solid surface. Part 1. Measurements before reaching the surface, J. Fluid Mech. 122 (1982) 57–89.
[18] Thole K.A., Bogard D.G., High freestream turbulence effects on turbulent boundary layers, J. Fluids Eng. 118 (1996) 276–284.
[19] Hunt J.C.R., Durbin P.A., Perturbed vortical layers and shear sheltering, Fluid Dyn. Res. 24 (1999) 375–404.
[20] Hunt J.C.R., Moin P., Lee M., Moser R.D., Spalart P., Mansour N.N., Kaimal J.C., Gaynor E., Cross correlation and length scales in turbulent flows near surfaces, in: Fernholz H.-H., Fiedler H.E. (Eds.), Advances in Turbulence 2, Springer-Verlag, 1989, pp. 128–134.
[21] Perot B., Moin P., Shear-free turbulent boundary layers. Part 1. Physical insights into near-wall turbulence, J. Fluid Mech. 295 (1995) 199–227.
[22] Schumann U., Minimum friction velocity and heat transfer in the rough surface layer derived from large eddy simulation, Bound.-Lay. Meteorol. 44 (1988) 311–326.
[23] Hunt J.C.R., Eddy dynamics and kinematics of convective turbulence, in: Plate E.J., Fedorovich E. (Eds.), Buoyant Convection in Geophysical Flows, Kluwer, Dordecht, 1998.
[24] Counihan J., Review paper. Adiabatic atmospheric boundary layers: a review and analysis of data from the period 1880–1972, Atmos. Environ. 9 (1975) 871–905.

[25] Cook N.J., On simulating the lower third of the urban boundary layer in a wind tunnel, Atmos. Environ. 7 (1973) 691–705.
[26] Lee M.J., Hunt J.C.R., The structure of sheared turbulence near a plane boundary, Proc. 7th Symposium on Turbulent Shear Flows, paper 8–1, 1989.
[27] Hunt J.C.R., Carruthers D.J., Rapid distortion theory and the 'problems' of turbulence, J. Fluid Mech. 212 (1990) 497–532.
[28] Wynngaard J.C., Cote O.R., Modelling buoyancy driven mixed layers, J. Atmos. Sci. 33 (1972) 1974–1988.
[29] Saddoughi S.G., Veeravalli S.V., Local isotropy in turbulent boundary layers at high Reynolds numbers, J. Fluid Mech. 268 (1994) 333–372.
[30] Perry A.E., Abell C.J., Scaling laws for pipe-flow turbulence, J. Fluid Mech. 67 (1975) 257–271.
[31] Perry A.E., Abell C.J., Asymptotic similarity of turbulence structures in smooth- and rough-walled pipes, J. Fluid Mech. 79 (1977) 785–799.
[32] Hunt J.C.R., Carlotti P., Spectra of Turbulence in Boundary Layers Near the Ground, Advances in Turbulence VIII, Kluwer Academic Publishers, 2000.
[33] Marušić I., Uddin A.K.M., Perry A.E., Similarity law for the streamwise turbulence intensity in zero-pressure-gradient turbulent boundary layers, Phys. Fluids 9 (1997) 3718–3726.
[34] Kline S.J., Reynolds W.R.C., Schraub F.A., Runstadler P.W., The structure of turbulent boundary layers, J. Fluid Mech. 30 (1967) 741–773.
[35] Brown G.L., Thomas A.S.W., Large structure in a turbulent boundary layer, Phys. Fluids Supplement 20 (1977) S243.
[36] Robinson S.K., The kinematics of turbulent boundary layer structure, NASA TM 103859, 1991.
[37] Morrison J.F., Bradshaw P., Burst and sources of pressure fluctuation in turbulent boundary layers, Proc. 8th Symposium on Turbulent Shear Flows, Paper 2–1, 1991.
[38] Mahrt L., Howell J.F., The influence of coherent structures and microfronts on scaling laws using global and local transforms, J. Fluid Mech. 260 (1994) 247–270.
[39] Jiménez J., Pinelli A., The autonomous cycle of near-wall turbulence, J. Fluid Mech. 389 (1999) 335–359.
[40] Klewicki J.C., Metzger M.M., Kelner E., Thurlow E.M., Viscous sublayer flow visualizations at $R_\theta \cong 1\,500\,000$, Phys. Fluids 7 (1995) 857–863.
[41] Fung J.C.H., Hunt J.C.R., Perkins R.J., Wray A.A., Stretch D., Defining the zonal structure of turbulence using the pressure and invariants of the deformation tensor, in: Johansson A.V., Alfredsson P.H. (Eds.), Advances in Turbulence 3, Springer-Verlag, 1991.
[42] Kim K.C., Adrian R. J., Very large-scale motion in the outer layer, Phys. Fluids 11 (1999) 417–422.
[43] Marušić I., Perry A.E., A wall-wake model for the turbulence structure of boundary layers. Part 2. Further experimental support, J. Fluid Mech. 298 (1995) 389–407.
[44] Zagarola M.V., Smits A.J., Mean-flow scaling of turbulent pipe flow, J. Fluid Mech. 373 (1998) 37–79.
[45] Katul G., Vidakovic B., The partitioning of attached and detached eddy motion in the atmospheric surface using Lorentz wavelet filtering, Bound.-Lay. Meteorol. 77 (1996) 153–172.
[46] Högström U., Analysis of turbulence structure in the surface layer with a modified similarity formulation for near neutral conditions, J. Atmos. Sci. 47 (1990) 1949–1972.
[47] Hoxey R.P., Richards P.J., Spectral characteristics of the atmospheric boundary layer near the ground, Proc. First UK Wind Engineering Society Conference, Cambridge, UK, 1992.
[48] Richards P.J., Hoxey R.P., Short J.L., Spectral models of the atmospheric surface layer, Proc. 10th International Conference on Wind Engineering, Copenhagen, 1999.
[49] Davenport A.G., The spectrum of horizontal gustiness near the ground in high winds, Q. J. Roy. Meteor. Soc. 87 (1961) 194–211.
[50] Colmer M.J., Measurements of horizontal windspeed and gustiness made at several levels on a 30 m mast, RAE Tech. Rept. 71214, 1971.
[51] Lauren M.K., Menabde M., Seed A.W., Austin G.L., Characterisation and simulation of the multiscaling properties of the energy-containing scales of horizontal surface-layer winds, Bound.-Lay. Meteorol. 90 (1999) 21–46.
[52] Fuehrer P.L., Friehe C.A., A physically-based turbulent velocity time series decomposition, Bound.-Lay Meteorol. 90 (1999) 241–295.
[53] Jiménez J., The largest scales of turbulent wall flows, Center for Turbulence Research, Annual Research Briefs, 1998, pp. 137–154.
[54] Williams D.R., Organized structures in the outer region of a turbulent pipe flow, MS Thesis, Dept. Mechanical and Aerospace Engineering, Princeton University, 1998.
[55] Fernholz H.-H., Finley P.J., The incompressible zero-pressure-gradient turbulent boundary layer: an assessment of the data, Prog. Aerosp. Sci. 32 (1996) 245–311.